Artifact level produced by different femoral head prostheses in CT imaging: diamond coated silicon nitride as total hip replacement material

Simone P. Rodrigues · José M. Paiva ·
Silvia De Francesco · Margarida I. Amaral ·
Filipe J. Oliveira · Rui F. Silva

Abstract Commercial femoral head prostheses (cobalt–chromium alloy, yttria partially stabilized zirconia (Y-PSZ) and alumina) and new silicon nitride ceramic ones (nanocrystalline diamond coated and uncoated) were compared in terms of artifact level production by computed tomography (CT). Pelvis examination by CT allows the correct diagnosis of some pathologies (e.g. prostate and colon cancer) and the evaluation of the prosthesis-bone interface in post-operative joint surgery. Artifact quantification is rarely seen in literature despite having a great potential to grade biomaterials according to their imaging properties. Materials' characteristics (density and effective atomic number), size and geometry of the prostheses can cause more or less artifact. A quantification procedure based on the calculation of four statistical parameters for the Hounsfield pixel values (mean, standard deviation, mean squared error and worst case error) is presented. CT sequential and helical scanning modes were performed. Results prove the artifact reproducibility and indicate that the cobalt–chromium and Y-PSZ are the most artifact-inducing materials, while alumina and silicon nitride (diamond coated and uncoated) ceramic ones present a low level of artifact. Considering the excellent biocompatibility and biotribological behaviour reported in earlier works, combined with the high medical imaging quality here assessed, diamond coated silicon nitride ceramics are arising as new materials for joint replacement.

S. P. Rodrigues (✉) · M. I. Amaral · F. J. Oliveira · R. F. Silva
CICECO, Department of Ceramics and Glass Engineering,
University of Aveiro, 3810-193 Aveiro, Portugal
e-mail: simonerodrigues@ua.pt

J. M. Paiva · S. De Francesco
Higher School of Health, University of Aveiro, 3810-193
Aveiro, Portugal

1 Introduction

The hip joint consists of two complementary articular surfaces—femoral head and acetabular cup—separated by cartilage and synovial fluid. This system is often clinically replaced by prostheses that ensure its functionality with an acceptable lifespan [1, 2]. Medical imaging plays an important role in the assessment of the prosthesis device-bone interface in post-operative hip joint replacement [3, 4]. It is also used for other clinical purposes such as guiding surgeries, diagnosing tumors, planning radiotherapy and identifying the spatial localization of pathological areas [5, 6]. Computed tomography (CT) is one of the most used imaging techniques due to high temporal resolution and detailed image at bone-tissue interfaces. Unfortunately, artifacts are inherent in CT images, affecting their quality and consequently the medical diagnosis [7]. An artifact is any feature that appears in an image and is not present in the original imaged object. For example, when materials of high atomic number and density exist implanted in the patient, e.g. hip prostheses, streak artifacts are generated in CT images due to photon absorption. Those artifacts along with image degradation hinder the ability to delineate tumors and certain organs, particularly in the case of treatment planning of prostate or colon cancer's patients who have undergone hip joint replacement. Artifacts can also obscure and be mistaken for pathology, resulting in false negatives and false positives. Although various methodologies and algorithms for artifact reduction in CT imaging have been developed [7–10], a simple and easy way to reduce CT artifact due to the presence of prostheses would be to use biomaterials that cause less X-ray attenuation. Therefore, patients with hip prostheses would have a chance of being diagnosed by CT imaging, without being subjected to high radiation doses, one of the methods used to reduce the artifacts.

In the present work, the artifact level produced by femoral head prostheses of cobalt–chromium alloy, yttria partially stabilized zirconia (Y-PSZ), alumina, and silicon nitride (diamond coated and uncoated), is quantified using the discrepancy between the Hounsfield CT numbers observed in the presence of those materials and the ones that would be obtained if they were not present. The first three femoral heads (cobalt–chromium alloy, Y-PSZ and alumina) are commercial and frequently used in joint replacement while the silicon nitride ceramics with and without diamond coating are new materials that have a high potential for this kind of application. Silicon nitride (Si_3N_4) ceramics emerged as a potential candidate for clinical applications because they are non-cytotoxic materials [11, 12] and present a reasonable fracture toughness, high wear resistance and low friction coefficient in most tribological systems [13, 14]. The Si_3N_4 ceramic enables bone growth around it [15] making it suitable for biomedical applications in articular joints like hip, knee, shoulder and spine [16, 17]. Although there are some studies demonstrating the superior wear resistance of this ceramic in hip joint simulator experiments [18], it was only very recently implanted by Amedica Corporation in hip and knee, and then, results that can prove their behaviour do not exist yet but the Amedica experts dared to say "We remain convinced that this new material will significantly improve clinical outcomes and implant longevity for patients who require joint replacement" [25].

In terms of biotribological behaviour, nanocrystalline diamond (NCD) coated silicon nitride ceramics present a wear rate in the range of 10^{-9} to 10^{-8} mm^3 N^{-1} m^{-1}, values that are similar to the best ones found for ceramic-on-ceramic combinations [19]. Furthermore, non-cytotoxic effects were observed and in vitro human osteoblast cell cultures revealed induced cell proliferation and stimulation of specific metabolic activities such ALP activity and matrix mineralization [20, 21], demonstrating the excellent biocompatibility of the NCD coated silicon nitride ceramics. This work will provide further information about the properties of these new materials, namely the imaging properties, and compare them with the materials in use for total hip replacement.

2 Materials and methods

2.1 Silicon nitride femoral heads manufacturing

Two silicon nitride (Si_3N_4) spheres with 28 mm diameter, provided with a cylindrical cavity to fit a Teflon stem, were home produced with the geometry and dimensional characteristics of the commercial femoral head prostheses used for comparison. The Si_3N_4 producing steps are described

below. The raw materials (AMPERPRESS Grade P, H·C. Starck) consisted of silicon nitride powder with sintering aids (aluminum oxide and yttrium oxide) and an organic binder adequate for ceramic green machining. Cylinder shaped blocks (40 mm diameter and 33 mm height) were uniaxial pressed at 160 MPa followed by machining in a CNC lathe to achieve the adequate sphere dimensions, assuming 1.225 of shrinking green-sintered constant. The compacts were burnt at 600 °C/4 h to remove the organic binder, followed by pressureless sintering in a conventional graphite furnace at 1750 °C/3 h in a nitrogen atmosphere. Surface finishing was firstly done by machining to adjust to final dimensions and then by manual polishing steps, using different grit sizes.

2.2 Nanocrystalline diamond film deposition

One of the two silicon nitride femoral heads was diamond coated by hot filament chemical vapour deposition (HFCVD). Prior to HFCVD, the sample surface was pre-treated, being 1 h abraded in ultrasonic (US) bath with a 6 nm sized diamond powder ethanol suspension and subsequently US cleaned in ethanol to remove the diamond loose particles. The NCD film was deposited using the following conditions: current intensity = 66A with 8 tungsten filaments horizontally disposed, CH_4/H_2 ratio = 0.02, total pressure = 25 mbar, filament temperature = 2100 °C, substrate temperature = 650 °C, gas flow = 100 ml/min and deposition time = 6 h.

2.3 Commercial femoral head prostheses

The commercial femoral heads used in the present work were obtained from LAFITT (CoCr alloy), ATF (alumina) and Morgan Technical Ceramics (Y-PSZ). Figure 1 shows the set of femoral head prostheses studied.

2.4 Experimental apparatus and procedure to CT image acquisition

The CT equipment used was a SOMATOM Sensation 64 Slice model from Siemens. In the experimental setup, CT images of each femoral head prostheses were acquired separately. It was used a big radiolucent plastic box (27.5 cm width, 38.5 cm length and 17.5 cm height dimensions) filled with water (attenuation coefficient similar to soft human tissues), Fig. 2a. An extra Teflon structure, fixed to a lateral side of the box, allowed positioning the Teflon stem at the center, holding the femoral head prosthesis, Fig. 2b. It is worth to note that this setup is responsible for the proper placement of the prosthesis inside the box, guaranteeing the same conditions of image acquisition, even when the prosthesis exchange is performed. This whole set of devices remained stable on the CT table, while the gantry moves
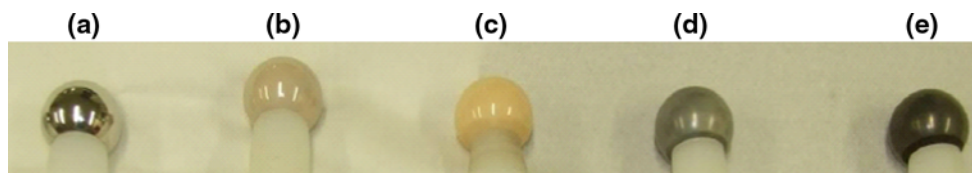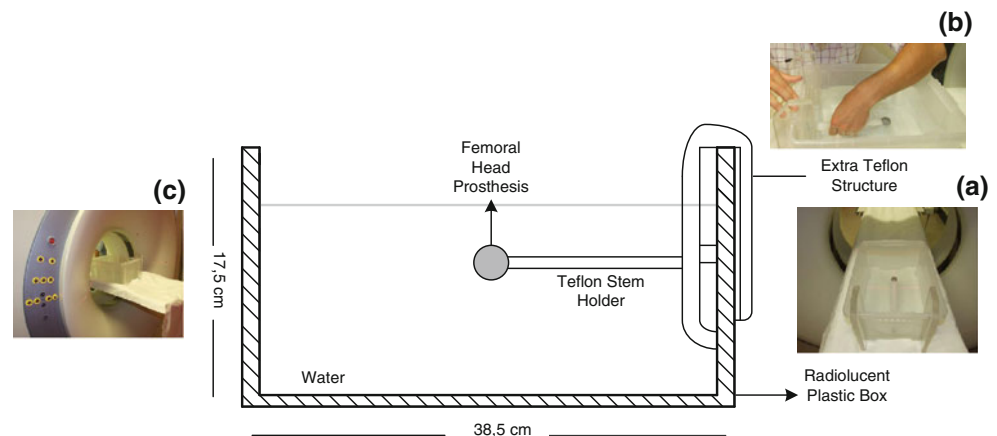
Fig. 1 The femoral head prostheses studied: (**a**) CoCr; (**b**) Y-PSZ; (**c**) alumina; (**d**) silicon nitride and (**e**) nanocrystalline diamond coated silicon nitride

Fig. 2 Experimental setup of the radiolucent plastic box used: (**a**) box on the static table; (**b**) prosthesis exchanging through and (**c**) the CT gantry imaging the femoral head prosthesis

itself to scan the object, Fig. 2c. The CT static table played an important role in avoiding water mass movement that would bring additional artifact. Prior to image acquisition, equipment alignment and centering was performed making use of a laser beam to guarantee that the submerged prosthesis was centered in its corresponding image. The scanning protocols, Table 1, used in this study were followed according to the manufacturer recommendations for the hip anatomy assessment. Three sequential (S-I to S-III) and four helical (H-I to H-IV) modes were used to evaluate the artifact. In the helical ones, the pitch was 0.90. The equipment ran at 120 kV, 150 mAs and 1 s rotation time.

2.5 Tests performed

Two evaluation tests were performed: the artifact reproducibility test, to evaluate if the artifact has always the same features and it is at the same position between two successive acquisitions; and, the material artifact comparison test, where the imaging properties of the different materials were measured and compared.

In the reproducibility test, sequential (S-I and S-II) and helical (H-I and H-II) scanning modes, described in Table 1, were twice performed. The sample used for the reproducibility test was the femoral head prosthesis of CoCr alloy which is supposed to produce more artifacts. In each operating mode (S-I, S-II, H-I and H-II), the comparison between the first and second acquisitions was done using the slice image corresponding to the biggest diameter of the prosthesis.

In the material artifact comparison test, two types of subtests were carried out: Test B31 and Test B60. The test designation is according to the filter used in the reconstruction of the image after data acquisition. The CT equipment used in this study allows choosing between a wide range of filters. Each filter is characterized by a value between 10 (softer) and 70 (more acute). The lower the value of the filter, the lower the noise of the reconstructed image but there are fewer details. Conversely, the higher the filter, the higher the image resolution but the amount of noise is larger. In this study, the two types of filters used, B31 and B60, are recommended by the manufacturer for the anatomical region under study: B31 is used for soft tissues and B60 for bone, where "B" indicates "body". In Test B31, S-I and H-I acquisition modes were performed, whereas in Test B60, S-III, H-III and H-IV operating conditions were chosen. As in the reproducibility test, the images intercepting the major prosthesis diameter were selected and further qualitatively and quantitatively compared.

2.6 Qualitative and quantitative evaluation methodology

In the CT reconstructed images, each pixel gives information about the coefficient of linear attenuation in Hounsfield Units (HU). All the images (512 × 512 pixels size) obtained in this study included pixels corresponding to air, water and prosthesis' presence, Fig. 3a.

Qualitative analysis was performed by the observation of the artifact's profile along one row and one column of the reconstructed image. The 128th row and the 128th

Table 1 Operating conditions used according to manufacturer (siemens) recommendations of the CT imaging equipment [24] for hip anatomy assessment (B31-soft tissues and B60-bone)

SOMATOM sensation 64 siemens	Sequential			Helical			
	S-I	S-II	S-III	H-I	H-II	H-III	H-IV
Acquisition parameters							
Acquisition (mm)	1×5	1×5	30×0.6	60×0.6	60×0.6	60×0.6	60×0.6
Slice collimation (mm)	5	5	0.6	0.6	0.6	0.6	0.6
Reconstruction process							
Slice thickness (mm)	5	5	3	5	5	3	0.75
Reconstruction interval (mm)	5	5	3	5	5	3	0.75
Filter	B31	B60	B60	B31	B60	B60	B60
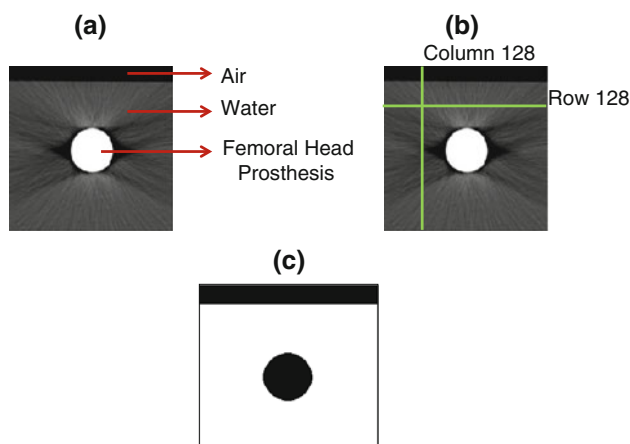
Fig. 3 (a) Type of CT image acquired; (b) placing of the 128th row and 128th column chosen to analyze the artifact profile and (c) the mask used to extract the water pixels

column were chosen, Fig. 3b, because both fit into a water region (with exception for the column's first 80 pixels that correspond to air) which have a theoretical value of zero HU for the coefficient of linear attenuation [22], if no artifacts are present. The plot of the HU values obtained in the presence of the prosthesis along these lines (2D graphs) gives qualitative information about the amplitude and location of the artifacts. Qualitative analysis was used to evaluate the artifact reproducibility and to compare the femoral head materials.

The quantification of artifacts can be made through the difference between the theoretical value in HU of the coefficient of linear attenuation for the region corresponding to water (0 HU) and the respective value when the prosthesis is present, being "error" the name given to that difference. Quantitative analysis was performed by using a mask to remove all the pixels of the water zone, Fig. 3c, and by calculating four statistical parameters, with Matlab[2009b] software, for the Hounsfield pixel values: mean value (M), standard deviation (SD), mean squared error (MSE) and worst case error (WCE). M is the average value of the pixels in HU, SD measures how much

dispersion there is from M, MSE is the average of the squares of the errors and WCE is the maximum value obtained for the error. Quantitative analysis was used to compare the imaging properties of the different femoral head materials.

3 Results

3.1 Artifact reproducibility test

Figures 4 and 5 show two consecutive CT images of the CoCr femoral head prosthesis and the corresponding artifact profiles along the 128th row and 128th column obtained for the operating conditions S-I/S-II and H-I/H-II, respectively. It can be seen that for sequential scanning mode, Fig. 4a–d, the artifact in the 1st image is identical to the one of the 2nd acquisition. This is confirmed by the observation of the artifact profiles once they overlap almost completely (Fig. 4e–h). When using helical scanning mode, Fig. 5a–d, the artifact does not replicate precisely the same profile between successive acquisitions. However, the artifact's shape and intensity are the same and only a very small region of the profiles does not match, Fig. 5e–h.

3.2 Material artifact comparison test

3.2.1 Test B31

Test B31 allows to compare all the different materials studied regarding their image quality in terms of artifact level, when using S-I and H-I scanning modes and a filter for soft tissues. The results of both modes were very similar and only S-I is depicted in Fig. 6 that shows the images of each prosthesis, (a–e), and their respective 128th row and 128th column artifact profiles, (f–i). The artifact profiles represented by the HU values obtained for each pixel placed along the 128th row and the 128th column are divided into two sets. A higher level of streak artifacts is easily seen across the entire image of cobalt–chromium (CoCr) and zirconia (Y-PSZ) than on alumina
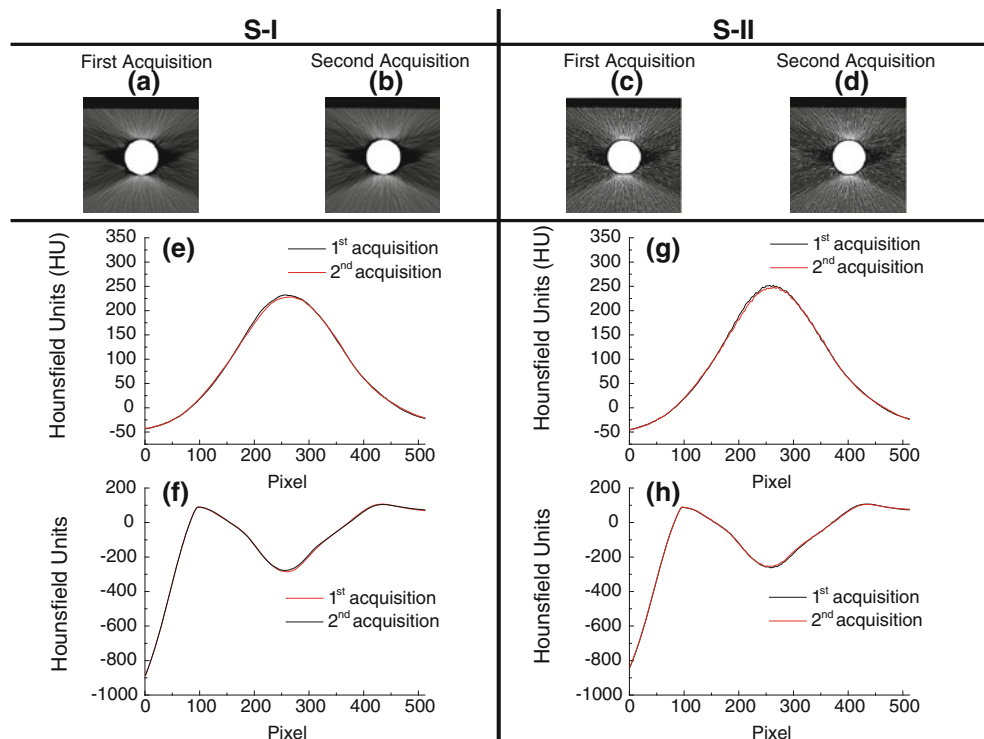
Fig. 4 Artifact reproducibility results using S-I and S-II operating conditions: (**a–d**) CT images of CoCr femoral head prosthesis; (**e**, **g**) the respective 128th row profiles; (**f**, **h**) the respective 128th column profiles


Fig. 5 Artifact reproducibility results using H-I and H-II operating conditions: (**a–d**) CT images of CoCr femoral head prosthesis; (**e**, **g**) the respective 128th row profiles; (**f**, **h**) the respective 128th column profiles
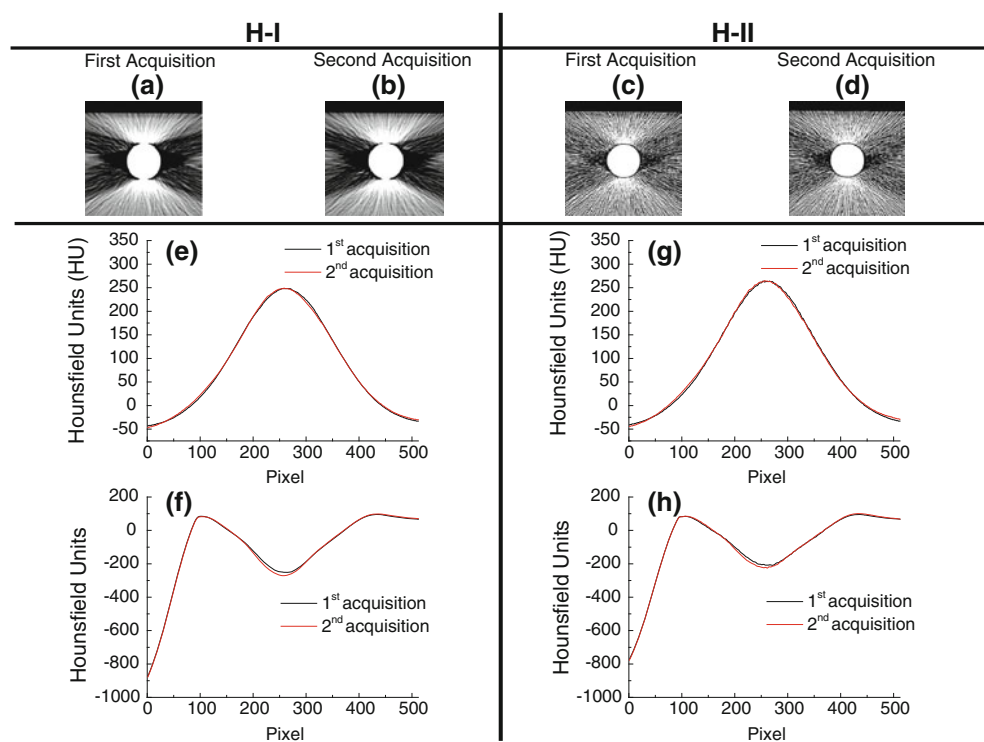
(Al_2O_3), silicon nitride (Si_3N_4) and nanocrystalline diamond coated silicon nitride (NCD/Si_3N_4) materials. Furthermore, the insertion cavity for stem is visualized only in the images of Al_2O_3, Si_3N_4 and NCD/Si_3N_4, which is related to the intrinsic properties of each material such as density and atomic number of the respective elemental composition. It is worth to note that the first 80 pixels plotted in the 128th column chart present negative HU values because they are located in an air region whose theoretical value for the coefficient of linear attenuation is -1000 HU. The profiles also evidence that the artifact is higher nearby the prostheses, which is heavily pronounced for CoCr and Y-PSZ.

Fig. 6 (**a–e**) Images obtained at Sequential I scanning mode for all materials studied; (**f, h**) their respective 128th row profiles; (**g, i**) their respective 128th column profiles
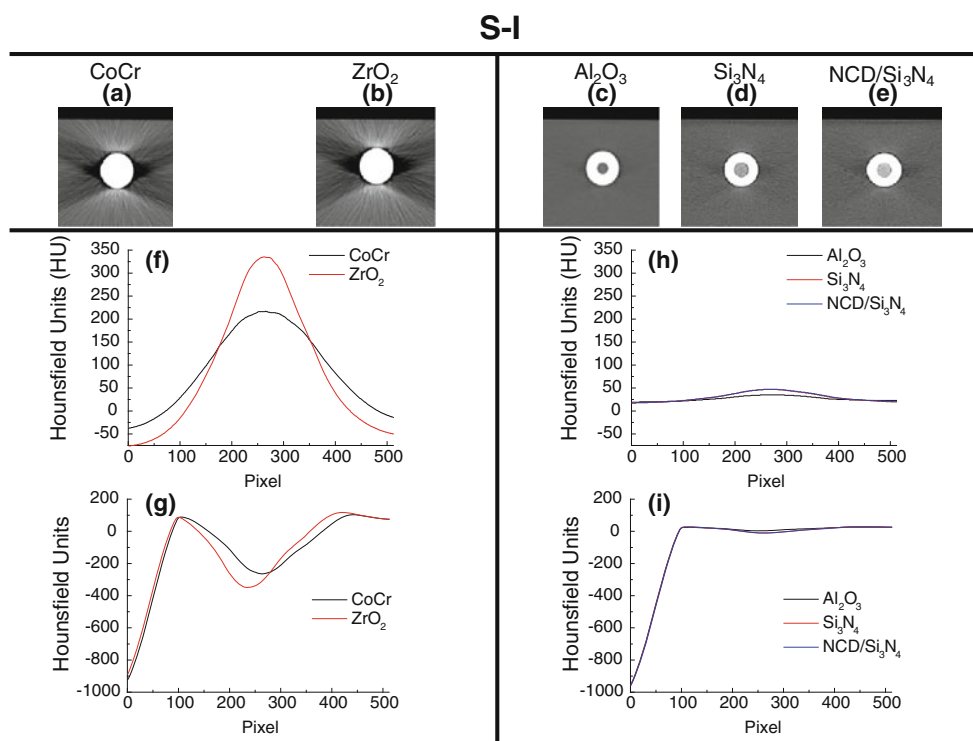
The artifact level was quantified using four statistical parameters: MSE, WCE, Mean and SD. For calculating these parameters only the water region pixels were taken into account. The respective values are showed in Fig. 7. It can be seen that Y-PSZ is the material that presents the highest WCE value (890 HU for S-I and 899 HU for H-I) while NCD/Si_3N_4 has the lowest (168 HU for S-I and 174 HU for H-I). Y-PSZ and CoCr present similar values regarding the other parameters, which are significantly higher than those of Al_2O_3, Si_3N_4 and NCD/Si_3N_4. Both scanning modes (S-I and H-I) generate similar statistical parameters and no significant differences are found between them.

3.2.2 Test B60

This subtest enables the comparison of all the materials studied regarding their image quality, when performing S-III, H-III and H-IV scanning modes and using a reconstruction filter for bone tissue. Results of all modes were very similar and only S-III is depicted in Fig. 8 that presents the CT images of the femoral head prostheses and the 128th row and 128th column artifact profiles.

Test B60 allows concluding again that CoCr and Y-PSZ produce more streak artifacts than Al_2O_3, Si_3N_4 and NCD/Si_3N_4. The insertion cavity for stem is still observed in Al_2O_3, Si_3N_4 and NCD/Si_3N_4 images and through the analysis of the artifact profiles one can conclude, once more, that these three ceramics show less deviation relatively to the theoretical value of water than Y-PSZ and CoCr.

The statistical parameters used to quantify the artifact level are showed in Fig. 7. The results follow the same trend as above described for Test B31.

4 Discussion

4.1 Artifact reproducibility test

To start the present study it was mandatory to ascertain the reproducibility of the artifact when successive acquisitions are performed with the same starting parameters. The reproducibility test was conducted using different operating conditions based on what is the usual practice to diagnose patients with hip prosthesis by CT imaging technique. Results have shown that for sequential scanning mode it is not possible to distinguish the artifact profiles of both acquisitions once they overlap almost completely, Fig. 4e–h, revealing that the artifact is reproducible. For the helical scanning mode, in the 128th column chart there is a small region of the artifact profiles that do not overlap. However, the intensity and the shape of the profiles are identical indicating that the mismatch is probably due to a small rotation caused by a different focus position at the beginning of the acquisition and not due to non-reproducibility of the artifact. This slightly change in the focus position introduces some adjustments in the data set used in the reconstruction of the image which gives rise to a non-matching area in the artifact profiles.
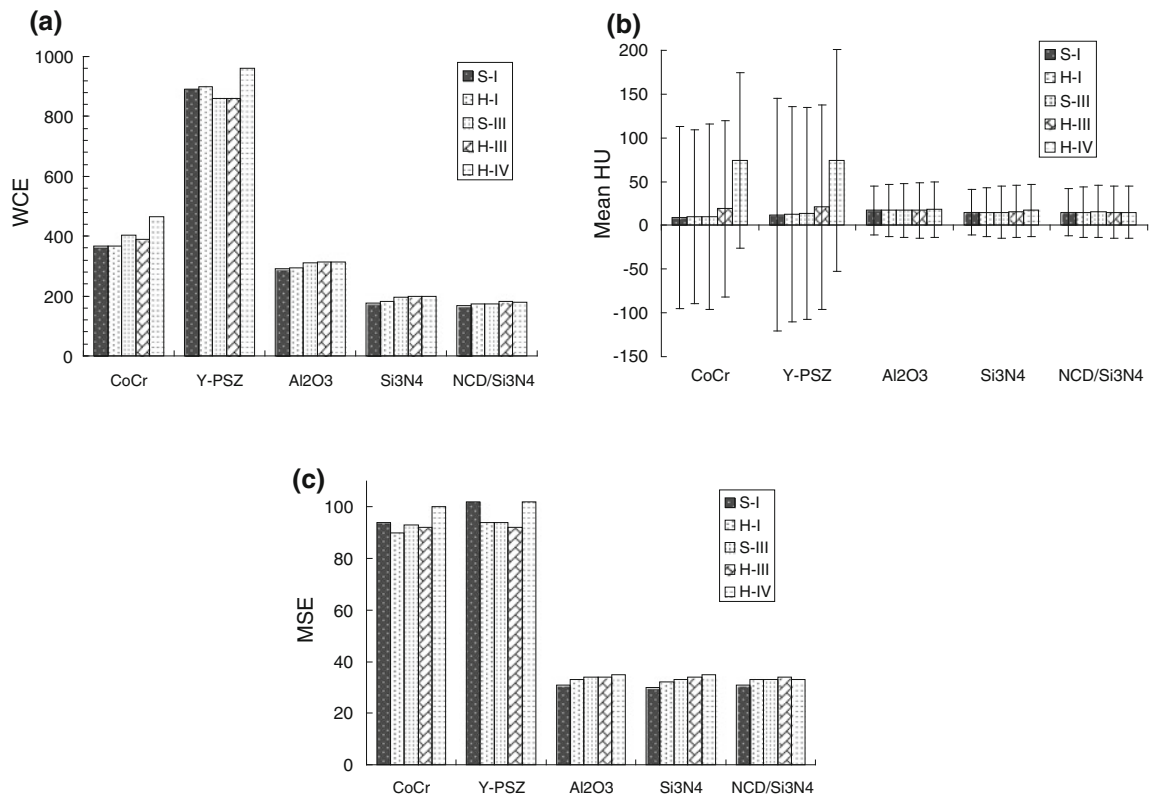
Fig. 7 Plotting of the statistical parameters calculated in order to quantify the image artifact produced by each prosthesis in CT imaging technique: (**a**) the worst case error; (**b**) mean and standard deviation and (**c**) mean squared error
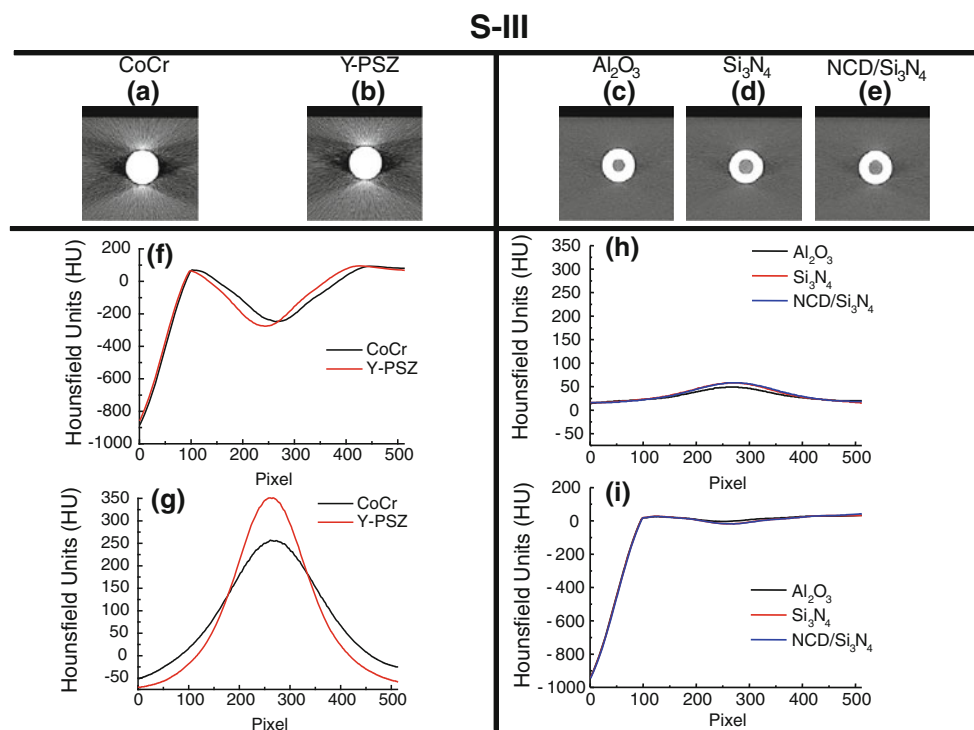

Fig. 8 (**a–e**) Images obtained at Sequential III scanning mode for all materials studied; (**f**, **h**) their respective 128th row profiles; (**g**, **i**) their respective 128th column profiles

Comparing the images of Figs. 4 and 5, it is visible that the helical scanning mode generates higher artifact level than the sequential one. This is often cited in the literature [7] and is related to the reconstruction process used that is not the same for both modes. Furthermore, it must be emphasized that the filters used in the reconstruction process interfere with the quality of the image which means that from S-I to S-II and from H-I to H-II, the images have more detail of the object in study but also more noise, which is perfectly seen in Figs. 4a–d and 5a–d.

In overall, the results of this test enable to assert the artifact reproducibility, either using the sequential or the helical scanning modes. Therefore, in the materials comparison test, it was performed only one acquisition per femoral head prosthesis.

4.2 Material artifact comparison test

In both tests, B31 and B60, a higher level of artifacts is visible for CoCr and Y-PSZ femoral head prostheses than for Al_2O_3, Si_3N_4 and NCD/Si_3N_4 ceramics. Furthermore, Y-PSZ has the highest value of WCE and NCD/Si_3N_4 presents the lowest, Fig. 7. At first sight, this is completely surprising because one expected that the CoCr femoral head prosthesis induces higher artifact level than Y-PSZ since it is metallic and has the highest physical density (8.2 g/cm^3 for CoCr and 6.1 g/cm^3 for Y-PSZ). However, the attenuation of the photon beam does not only depend on the physical density of the object to be imaged but also on the atomic number of the elemental composition [23]. The effective atomic number of zirconia (35.7) is higher than the one of CoCr (27.7) which may explain the highest WCE value.

Among the set of materials tested, Al_2O_3, Si_3N_4 and NCD/Si_3N_4 are the less attenuating materials enabling a correct object reconstruction with slightly artifact visualization. These two materials, alumina (Al_2O_3) and silicon nitride (Si_3N_4) are ceramic compounds with low physical densities ($Al_2O_3 = 3.9$ g/cm^3; $Si_3N_4 = 3.2$ g/cm^3) as well as low effective atomic numbers ($Al_2O_3 = 11.1$; $Si_3N_4 = 12.1$) and for that reason are the ones that induce the lowest artifact level. The diamond film that coats the silicon nitride femoral head (NCD/Si_3N_4) does not modifies significantly the image quality when compared to the ceramic uncoated (Si_3N_4), although the WCE values of NCD/Si_3N_4 are slightly lower than the ones of Si_3N_4, as seen in Fig. 7.

The mean values (M) should be close to zero in materials that would ideally show less artifact level (Al_2O_3, Si_3N_4 and NCD/Si_3N_4) and a bit higher in materials that present intense artifacts (CoCr and Y-PSZ). However, the values of M obtained are similar for all the materials studied. In the cases where the artifact level is more pronounced (CoCr and Y-PSZ), the positive and negative HU pixel values compensate themselves resulting in a mean value closer to zero than the one calculated for materials with an artifact less pronounced (Al_2O_3, Si_3N_4 and NCD/Si_3N_4). Standard deviation, although, is higher for CoCr and Y-PSZ than for Al_2O_3, Si_3N_4 and NCD/Si_3N_4, revealing a bigger dispersion of values for the first two materials and indicating that despite having the lowest average pixel values, these are located in a larger range which means higher artifact levels.

The MSE values are more appropriate parameters to ascertain the artifact level than the M ones. In Fig. 7, one can see clearly two ranges of MSE values, 90–102 and 27–35, dividing the materials into groups: the most (CoCr and Y-PSZ) and less artifact-inducing (Al_2O_3, Si_3N_4 and NCD/Si_3N_4), respectively, confirming the trend that was observed for the 128th row and 128th column artifact profiles and for the WCE parameter.

With respect to the variation of the artifact level with the operating conditions, no significant differences were found for the two filters used. However, the H-IV scanning mode seems to present a higher artifact level than the S-III and H-III conditions, for the same filter (B60). This is related with the slice thickness of the image acquisition which is the smallest (0.75 mm) used in the present work.

5 Conclusions

The imaging properties of five different femoral head prostheses (cobalt–chromium alloy, yttria partially stabilized zirconia (Y-PSZ), alumina and diamond coated and uncoated silicon nitride) were characterized by CT imaging technique. The quality of the images was evaluated in terms of artifact level produced in the presence of different materials. This level was quantified using four statistical parameters calculated for the pixel values of the coefficient of linear attenuation in Hounsfield Units (HU).

Prior to the materials comparison test it was necessary to confirm the reproducibility of the artifact between successive acquisitions. It was found that the artifact is reproducible both in sequential as in helical scanning modes. Therefore, one acquisition per material is sufficient for ascertain the artifact level and thus to compare materials.

The cobalt–chromium (CoCr) and Y-PSZ femoral head prostheses are the ones that induce the highest artifact levels. On the contrary, alumina (Al_2O_3), silicon nitride (Si_3N_4) and nanocrystalline diamond coated silicon nitride (NCD/Si_3N_4) exhibit low levels of artifact of which the NCD/Si_3N_4 is the best, having the lowest WCE value. These imaging properties added to the fact that the nanocrystalline diamond film deposited on a silicon nitride ceramic substrate enhances the wear resistance and exhibits excellent biocompatibility with induced osteoblast proliferation; make it an excellent choice for total hip replacement.

References

1. Santavirta S, Böhler M, Harris WH, Konttinen YT, Lappalainen R, Muratoglu O, et al. Alternative materials to improve total hip replacement tribology. Acta Orthop Scand. 2003;74(4):380–8.
2. Navarro M, Michiardi A, Castaño O, Planell JA. Biomaterials in orthopaedics. J R Soc Interface. 2008;5:1137–58.
3. Berg BV, Malghem J, Maldague B, Lecouvet F. Multi-detector CT imaging in the postoperative orthopedic patient with metal hardware. Eur J Radiol. 2006;60:470–9.
4. Mitsuhashi S, Harada Y, Yanagawa N, Kamikawa K, Kitahara H, Moriya H. Automatic measurement of polyethylene modification in metal-backed artificial hip joints using three-dimensional CT. J Orthop Sci. 2004;9(1):10–5.
5. Aubin M, Morin O, Chen J, Gillis A, Pickett B, Aubry JF, et al. The use of megavoltage cone-beam CT to complement CT for target definition in pelvic radiotherapy in the presence of hip replacement. Br J Radiol. 2006;79:918–21.
6. Yazdia M, Gingras L, Beaulieu L. An adaptative approach to metal artifact reduction in helical computed tomography for radiation therapy treatment planning: experimental and clinical studies. Int J Radiat Oncol Biol Phys. 2005;62(4):1224–31.
7. Barret JF, Keat N. Artifacts in CT: recognition and avoidance. RadioGraphics. 2004;24:1679–91.
8. Liu PT, Pavlicek WP, Peter MB, Spangehl MJ, Roberts CC, Paden RG. Metal artifact reduction image reconstruction algorithm for CT of implanted metal orthopedic devices: a work in progress. Skelet Radiol. 2009;38:797–802.
9. Man BD, Nuyts J, Dupont P, Marchal G, Suetens P. Reduction of metal streak artifacts in X-ray computed tomography using a transmission maximum a posteriori algorithm. IEEE Trans Nucl Sci. 2000;47(3):977–81.
10. Robertson DD, Yuan J, Wang G, Vannier MW. Total hip prosthesis metal-artifact suppression using iterative deblurring reconstruction. J Comput Assist Tomogr. 1997;21(2):293–8.
11. Mazzocchi M, Bellosi A. On the possibility of silicon nitride as a ceramic for structural orthopaedic implants. Part I: processing, microstructure, mechanical properties, cytotoxicity. J Mater Sci Mater Med. 2008;19:2881–7.
12. Neumann A, Reske T, Held M, Jahnke K. Comparative investigation of the biocompatibility of various silicon nitride ceramic qualities in vitro. J Mater Sci Mater Med. 2004;15:1135–40.
13. Abreu CS, Oliveira FJ, Belmonte M, Fernandes AJS, Gomes JR, Silva RF. CVD diamond coated silicon nitride self-mated systems: tribological behaviour under high loads. Tribol Lett. 2006;21(2):141–51.
14. Amaral M, Abreu CS, Fernandes AJS, Oliveira FJ, Gomes JR, Silva RF. Nanodiamond-based tribosystems. Surf Coat Technol. 2010;204:1962–9.
15. Guedes e Silva CC, König B, Carbonaric MJ, Yoshimoto M, Allegrini S, Bressiani JC. Bone growth around silicon nitride implants—an evaluation by scanning electron microscopy. Mater Charact. 2008;59:1339–41.
16. Bal BS, Rahaman MN. Orthopedic applications of silicon nitride ceramics. Acta Biomater. 2012;8:2889–98.
17. Sonntag R, Reinders J, Kretzer JP. What's next? Alternative materials for articulation in total joint replacement. Acta Biomater. 2012;8:2434–41.
18. Bal BS, Khandkar A, Lakshminarayanan R, Clarke I, Hoffman AA, Rahaman MN. Fabrication and testing of silicon nitride bearings in total hip arthroplasty: winner of the 2007 "HAP" PAUL Award. J Arthroplast. 2009;24(1):110–6.
19. Amaral M, Abreu CS, Oliveira FJ, Gomes JR, Silva RF. Tribological characterization of NCD in physiological fluids. Diam Relat Mater. 2008;17:848–52.
20. Amaral M, Gomes PS, Lopes MA, Santos JD, Silva RF, Fernandes MH. Nanocrystalline diamond as a coating for joint implants: cytotoxicity and biocompatibility assessment. J Nanomater. 2008;2008:1–9.
21. Amaral M, Gomes PS, Lopes MA, Santos JD, Silva RF, Fernandes MH. Cytotoxicity evaluation of nanocrystalline diamond coatings by fibroblast cell cultures. Acta Biomater. 2009;5:755–63.
22. Kim HK, Kum O, Max NL. Computer-aided CT image analysis based on clustered hounsfield values. J Korean Phys Soc. 2007;51(1):235–44.
23. Coolens C, Childs PJ. Calibration of CT Hounsfield units for radiotherapy treatment planning of patients with metallic hip prostheses: the use of the extended CT-scale. Phys Med Biol. 2003;48(1591):1603.
24. Siemens (2005) AG Medical Solutions—Somatom sensation 40/64 application guide.
25. Seredy C, Zeiger S, AMEDICA/US SPINE® Enters the reconstructive surgery market—First silicon nitride total hip replacement. http://amedica.com/company/news/02.17.11.pdf. Accessed July 2011.